

Article

Simplified Modelling Techniques for Dynamic Wireless Power Transfer

Krzysztof Jakubiak ^{1,*}, Jun Liang ¹, Liana Cipcigan ¹, Chuanyue Li ¹ and Jingzhe Wu ²

¹ School of Engineering, Cardiff University, Cardiff CF10 3EU, UK; liangj1@cardiff.ac.uk (J.L.); cipciganlm@cardiff.ac.uk (L.C.); lic23@cardiff.ac.uk (C.L.)

² Continental Automotive Systems, Auburn Hills, MI 48326, USA; jingzhe.wu@continental-corporation.com

* Correspondence: jakubiaks@cardiff.ac.uk

Abstract: Recent advancements in Dynamic Wireless Power Transfer (DWPT) have highlighted the need for further research, particularly in the area of modelling and simulation techniques. As the power transferred between charging pads depends on vehicle position, the load profile of the DWPT is therefore a function of the vehicle's movement which is dependent on user behaviour and is inherently stochastic. For DWPT, these events involve high instantaneous power and are short in duration. To better understand the impact of DWPT, accurate models are required to test control systems and potential solutions. Additionally, these systems require high-frequency simulation for DWPT, which results in long simulation times during development. This paper presents a simplified model for circuit components that eliminates high-frequency switching elements, enabling the use of larger simulation time steps and significantly reducing simulation time. By applying circuit analysis and calculating equivalent impedances, the model provides average circuit values that effectively represent waveform amplitudes without the need to simulate instantaneous, high-frequency variations. To ensure the efficiency of grid-connected simulations and achieve a level of accuracy that reflects the internal dynamics of wireless charging, subsystem simulations demonstrated significant time improvements at the cost of minimal accuracy loss. For DC/DC converters operating at 2 kHz, simulation time was reduced by 3× with only a 1% error. The DWPT subsystem, operating at 85 kHz, achieved an 18× reduction in simulation time with a 2.5% deviation. When combined, the full system resulted in a 30-fold reduction in simulation time with only a 6% deviation from the base model.



Citation: Jakubiak, K.; Liang, J.; Cipcigan, L.; Li, C.; Wu, J. Simplified Modelling Techniques for Dynamic Wireless Power Transfer. *Electronics* **2024**, *13*, 4300. <https://doi.org/10.3390/electronics13214300>

Academic Editor: Fabio Corti

Received: 13 September 2024

Revised: 24 October 2024

Accepted: 26 October 2024

Published: 31 October 2024



Copyright: © 2024 by the authors. Licensee MDPI, Basel, Switzerland. This article is an open access article distributed under the terms and conditions of the Creative Commons Attribution (CC BY) license (<https://creativecommons.org/licenses/by/4.0/>).

Keywords: dynamic wireless power transfer; wireless power transfer; electric vehicles; dynamic wireless charging; mutual inductance; system modelling; high-frequency simulation; wireless charging; system modelling

1. Introduction

The global effort to reduce greenhouse gases (GHGs) emissions has identified road transportation as a major contributor [1]. Consequently, Electric Vehicles (EVs) have seen increased adoption as part of the transition to greener energy sources, aiming to eliminate tailpipe emissions. The main issues for EVs stem from the use of a battery offering a lower driving range (compared to Internal Combustion Engine (ICE) vehicles) and the limited availability of charging solutions. Some of the main issues facing EVs are the driving range (compared to ICE vehicles) and insufficient charging infrastructure [2]. DWPT aims to extend the driving range by providing continuous charging opportunities that are accessible by multiple users. Wireless charging as a solution offers a better user experience and eliminates interoperability issues [3]. The stationary requirement placed on conductive charging is no longer present as a power transfer no longer requires a physical connection. Dynamic Wireless Charging (DWC) offers an opportunistic charging approach, where any vehicle can be charged while driving over a DWC coil. Research on compensation

topologies, coil design and control have been previously covered to guide the design process [4–11]. Calculating the mutual inductance between coils depends on the position, orientation shape and size of the coils [12–20].

With short high-power energy bursts, the grid connections require more research to better understand the impact of adopting DWC. Further investigating the effects with larger adoption rates would require more simulation analyses, which becomes a computational issue as each set of coils runs at 85 kHz. While a detailed simulation might be necessary to run for design and control purposes, this is less necessary for grid interaction studies, as such, these more complicated systems are summarised by load profiles that aim to give a general idea of behaviour based on power consumption [21–26]. From these load profiles, high-level observations can be made as a first step in order to gain a better understanding of the interaction and explore possible control strategies, as a load profile speaks only to the power consumption based on time, which is not necessarily specific to the DWC system.

There are different ways to both design and control Wireless Power Transfer (WPT) systems depending on load and objectives for the system. Most commonly, the series-series compensation is used for its power transfer capability while having efficiency independent of the coupling factor. For the purpose of grid interaction, dual-sided control is recommended to allow for the control and ripple reduction in both grid and load current fluctuations [27,28]. For system-equivalent models, a series of equivalent models are used [29]. While the coupling between two coils has previously been discussed, it remains a property specific to the designed circuit [12], whereby either a coupling factor or mutual inductance can be used. Updating this property achieves dynamic operation of the system.

At present, there is a lack of simulation techniques specifically tailored for DWPT, as most rely on static WPT simulations and design methods that do not fully capture the dynamic behaviour of the system. This becomes critical when considering grid interaction studies, where accurately capturing system dynamics and responses to various factors is essential. Due to the high-frequency operation of DWPT, integrating a single charging system into grid simulations adds complexity. Future grid interaction studies will involve multiple primary-side transmitter coils and multiple receiver coils, further increasing system complexity. While the primary focus for both the grid and the vehicle is on power transfer characteristics, there is an opportunity to simplify existing models and still provide accurate representations of power consumption from the grid and power transferred to the vehicle. Therefore, this paper analyses the DWPT system using a state-space representation with equivalent impedance to capture system dynamics without the need for high-frequency switching.

Section 2 describes the switching system (and its operation mechanism), which is used as a baseline for the proposed system in Section 3, which details the equations used for modelling the simplifying DWC system. Section 4 presents the results of the proposed system and discusses implementation accuracy and speed trade-off.

2. Dynamic Wireless Charging Switching Circuit

2.1. Full Circuit

The basic system required for WPT for EVs charging the minimum circuit required consists of an inverter, rectifier, inductive coils and compensation capacitors. Adding primary and secondary DC/DC converters helps to improve the efficiency and control of the system by decoupling both the source and load from fluctuations in the wireless power transfer system.

The base circuit used for comparison in this research is shown in Figure 1. The sub-circuit function aims to control either the voltage or current at the intersection or connection points between subsystems. The primary-side DC/DC converter controls the DC bus voltage, which is supplied to the inverter. The inverter controls the switching frequency for WPT based on system parameters that result in a secondary coil current. The controlled rectifier using a secondary coil current maintains a reference DC voltage.

Finally, the secondary DC converter can be set to constant current or voltage based on load requirements (for EVs, this is based on State-of-Charge (SOC)).

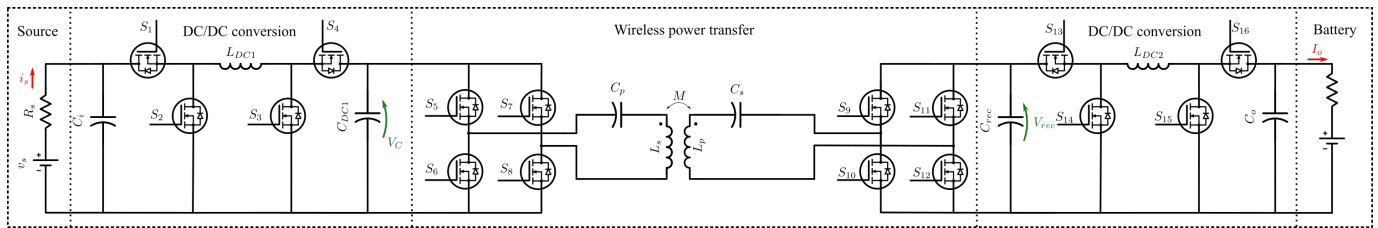


Figure 1. Full system schematic.

Note: The circuit is designed to be symmetrical around the inductive coils, and hence can be configured to run in reverse mode for vehicle-to-grid (V2G) applications

2.2. DC/DC Converter

For both the primary and secondary sides of the circuit in Figure 1, a configurable bidirectional DC/DC converter is used as shown in Figure 2. Based on the use of switches S₁–S₄, the converter can be set to buck, buck–boost or boost mode in either forward or reverse direction. The possible configurations are shown in Table 1, where a PWM signal is used to track a reference signal using a PI controller.

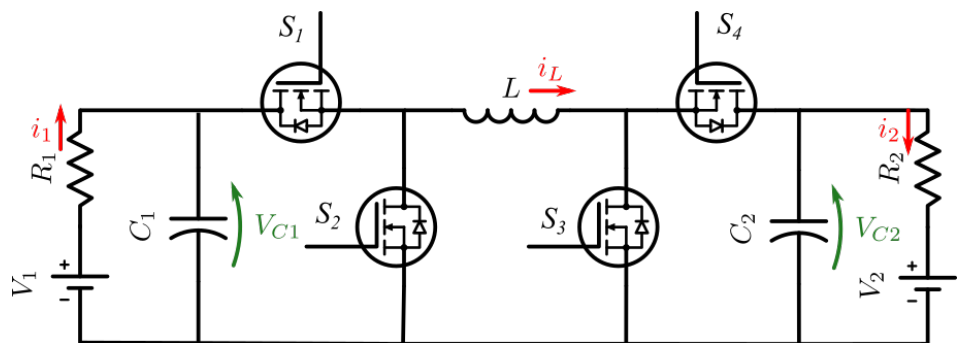


Figure 2. Configurable bidirectional DC/DC converter.

Table 1. DC/DC converter configurations.

Mode	S ₁	S ₂	S ₃	S ₄
Buck	PWM	0	0	0
Buck–Boost	PWM	0	PWM	0
Boost	1	0	PWM	0
Reverse Buck	0	0	0	PWM
Reverse Buck–Boost	0	PWM	0	PWM
Reverse Boost	0	PWM	0	1

2.3. Inverter

A fixed duty cycle inverter is used to drive the WPT circuit at resonant frequency. Figure 3 shows a basic implementation where a constant voltage source and restive load are shown for circuit simplicity; these are later replaced with the circuits shown in Figure 1.

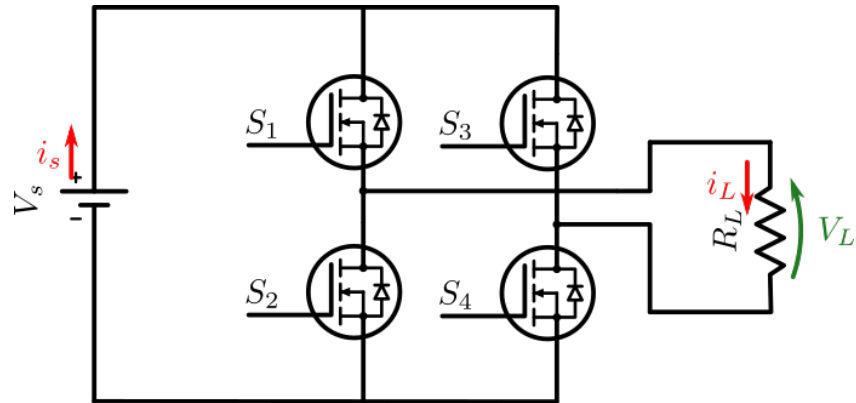


Figure 3. Inverter diagram.

2.4. Dynamic Wireless Power Transfer

The DWPT model relates the two inductive coils using the induced voltage, which is a function of mutual inductance. Other mutual inductance systems such as fixed-core transformers also use the same approach. The mutual inductance is a parameter which describes the link between both primary and secondary sides; the coupling factor is a unit-less constant that describes the same relationship (coupling factor $k = M/\sqrt{L_1L_2}$).

The remainder of the circuit (Figure 4) uses series-series-connected compensation for resonant operation, and an equivalent load resistance is used for the diagram. The DWPT model only requires measuring i_1 and i_2 to generate the induced voltages (shown as sMi_1 and $-sMi_2$). Hence, the source and load can be connected to the full circuit without changing the DWPT.

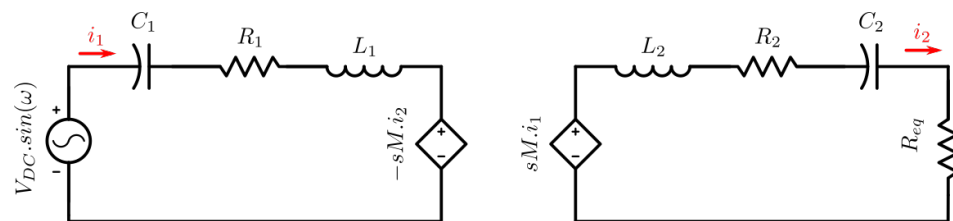


Figure 4. WPT model.

Finally, dynamic modelling is achieved by varying the mutual inductance variable. As the mutual inductance is a function of displacement between the two coils, changing the mutual inductance will model the dynamic changes in the system. Previous research discusses this in more detail [27], including the model used for mutual inductance [12].

2.5. Semi-Controlled Rectifier

Figure 5 shows the model used for the semi-active rectifier, only switches S2 and S4 are used to control the power flow. When $S2 = S4 = 0$, this functions as a rectifier allowing for maximum power flow; when $S2 = S4 = 1$, a return path is created for the source current, effectively disconnecting the power flow.

The use of this circuit is recommended as a secondary DC voltage source can keep rising throughout the operation up to an unsafe level. This occurs when the WPT provides more power than is passed to the load, which occurs often when providing constant output characteristics and will also have an impact on output voltage/current ripple. The alternative is to introduce further control into the system where, typically at the primary side, there is a delay in the response as a secondary DC/DC voltage is decoupled from the primary converters by the WPT circuit. Furthermore, the practicality of having primary/secondary-side communication can be an issue.

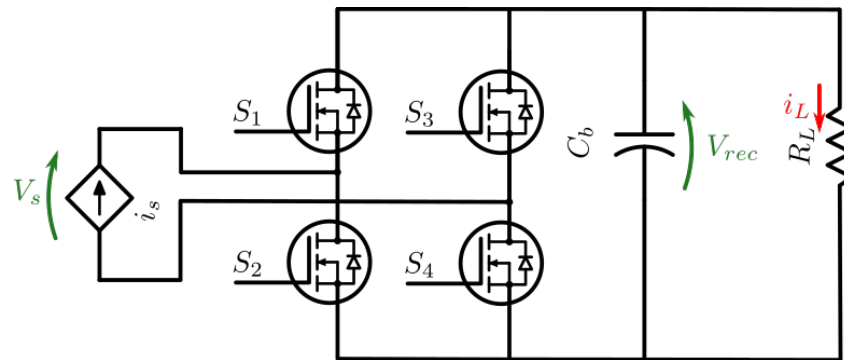


Figure 5. Semi-controlled rectifier diagram.

2.6. System Control

The circuit used in Figure 1 is designed to have each subsystem's control variables within its circuit using a PI controller for a duty cycle, which is then used to generate a PWM signal supplied to the switches as described in each sub-circuit section above. Hence, the primary DC/DC converter controls the primary DC bus voltage; the inverter is fixed to a duty cycle (hence, uncontrolled); the rectifier controls the secondary DC bus voltage; and the secondary DC/DC converter controls the load charging characteristics (the constant current used in this paper).

2.7. Connection of Subsystems and Additional Requirements

The interconnection of subsystems can be a challenge, as ideally, these systems would connect directly to each other (similar to the switching circuit). However, this is not always possible as each system is designed with ideal sources and loads; hence, a solution can be achieved. Once multiple systems are chained together, the MATLAB Simulink R2023a solver faces issues in defining circuit parameters and views the system as a logic loop.

2.7.1. Primary DC/DC Converter

The main consideration for this circuit is the conversion of the primary coil current from WPT to the equivalent DC current to be applied to the output of the DC/DC converter. The relationship between the magnitude of primary coil current (I_p) and primary DC/DC converter output current ($I_{2_{DC1}}$) can be determined via the following:

$$I_{2_{DC1}} = \eta I_p / \sqrt{2} \approx 0.64 I_p \quad (1)$$

where η is the converter efficiency. This is an approximation. Assuming that the converter voltage drop is negligible, the remainder converts the WPT model's value to an RMS value.

2.7.2. Wireless Power Transfer

First, the implementation for WPT assumes a sinusoidal input voltage; as the voltage applied in this study is a square wave, the approximate value for the input voltage is given by

$$V_{in_{WPT}} \approx 1.27 V_{2_{DC1}} \quad (2)$$

This is implemented in code which is USED FOR as shown in Appendix B.

Next, the implementation uses a small signal approach, which has been converted to equivalent impedance. While the equations are preserved, note the scale factor (sf) applied in the code to scale up the state space implementation response time.

Approximating the load resistance (secondary DC/DC converter) is achieved by approximating the converter's power consumption:

$$R_L = \begin{cases} 4 \times 10^3, & \text{if } k < 0 \\ R_{DCDC2}, & \text{otherwise} \end{cases} \quad (3)$$

where,

$$R_{DCDC2} = 0.5d_{rec} \frac{V_{rec}}{i_o V_o} \quad (4)$$

and where d_{rec} is the duty cycle applied to the semi-active rectifier.

Finally, approximating the rectifier voltage (V_{Rec}) is performed as a function of both the secondary coil current (I_s) and converter-equivalent resistance (R_{DCDC2}), such that

$$C_{Rec} \frac{dV_{rec}}{dt} = \sqrt{2}d_{rec}I_s - \frac{V_{Rec}}{R_{DCDC2}} \quad (5)$$

2.7.3. Secondary DC/DC Converter

Once the considerations above are implemented, the circuit can be used the same as shown in the analysis by applying rectifier voltage (V_{Rec}).

3. Circuit Equations and Equivalent Circuits

3.1. DC/DC Converter

Figure 2 shows the bidirectional DC/DC converter. To achieve forward operation mode, $S_2 = S_4 = 0$, leaving S_1 as the buck control switch and S_3 as the boost control switch, thus allowing the use of buck mode ($S_1 = PWM, S_3 = 0$), boost mode ($S_1 = 1, S_3 = PWM$), or buck–boost mode ($S_1 = S_3 = PWM$). The same is possible for the reverse operation mode, where $S_1 = S_3 = 0$, buck mode ($S_4 = PWM, S_2 = 0$), boost mode ($S_4 = 1, S_2 = PWM$), or buck–boost mode ($S_2 = S_4 = PWM$). Carrying out the circuit analysis gives the following:

3.1.1. Buck Mode

$$\frac{dv_{c1}}{dt} = \frac{i_1}{C_1} - d \frac{i_L}{C_1} \quad (6)$$

$$\frac{di_L}{dt} = d \frac{v_{c1}}{L} - \frac{v_{c2}}{L} \quad (7)$$

$$\frac{dv_{c2}}{dt} = \frac{i_L}{C_2} - \frac{i_2}{C_2} \quad (8)$$

3.1.2. Buck–Boost Mode

$$\frac{dv_{c1}}{dt} = \frac{i_1}{C_1} - d \frac{i_L}{C_1} \quad (9)$$

$$\frac{di_L}{dt} = d \frac{v_{c1}}{L} - (1-d) \frac{v_{c2}}{L} \quad (10)$$

$$\frac{dv_{c2}}{dt} = (1-d) \frac{i_L}{C_2} - \frac{i_2}{C_2} \quad (11)$$

3.1.3. Boost ModeReverse

$$\frac{dv_{c1}}{dt} = \frac{i_1}{C_1} - \frac{i_L}{C_1} \tag{12}$$

$$\frac{di_L}{dt} = \frac{v_{c1}}{L} - (1-d)\frac{v_{c2}}{L} \tag{13}$$

$$\frac{dv_{c2}}{dt} = (1-d)\frac{i_L}{C_2} - \frac{i_2}{C_2} \tag{14}$$

3.1.4. Buck ModeReverse

$$\frac{dv_{c1}}{dt} = \frac{i_1}{C_1} - \frac{i_L}{C_1} \tag{15}$$

$$\frac{di_L}{dt} = \frac{v_{c1}}{L} - d\frac{v_{c2}}{L} \tag{16}$$

$$\frac{dv_{c2}}{dt} = d\frac{i_L}{C_2} - \frac{i_2}{C_2} \tag{17}$$

3.1.5. Buck–Boost ModeReverse

$$\frac{dv_{c1}}{dt} = \frac{i_1}{C_1} - (1-d)\frac{i_L}{C_1} \tag{18}$$

$$\frac{di_L}{dt} = (1-d)\frac{v_{c1}}{L} - d\frac{v_{c2}}{L} \tag{19}$$

$$\frac{dv_{c2}}{dt} = d\frac{i_L}{C_2} - \frac{i_2}{C_2} \tag{20}$$

3.1.6. Boost ModeReverse

$$\frac{dv_{c1}}{dt} = \frac{i_1}{C_1} - (1-d)\frac{i_L}{C_1} \tag{21}$$

$$\frac{di_L}{dt} = (1-d)\frac{v_{c1}}{L} - \frac{v_{c2}}{L} \tag{22}$$

$$\frac{dv_{c2}}{dt} = \frac{i_L}{C_2} - \frac{i_2}{C_2} \tag{23}$$

The equivalent model of the DC/DC converter can be seen in Figure 6 and its Simulink implementation is shown in Figure 7.

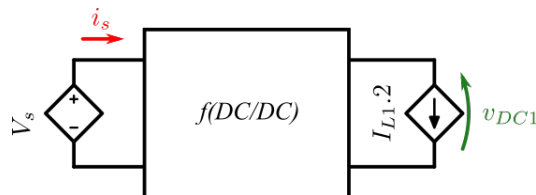


Figure 6. DC/DC-equivalent circuit.

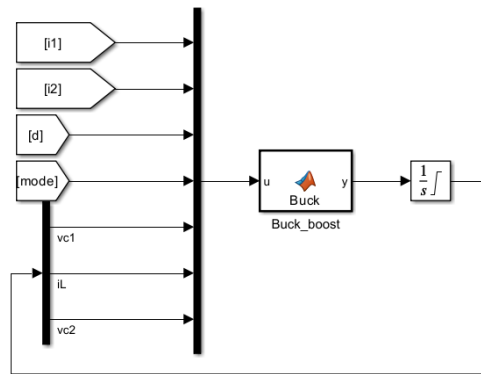


Figure 7. The DC/DC converter’s Simulink implementation.

3.2. Inverter

For the purpose of this research, a fixed duty cycle is used to generate a square wave with amplitude $\pm V_{DC}$. The supply voltage/current can hence be related to its load voltage/current, given by

$$V_{source} = |V_{load} - 2R_{fet} * I_{load}| \tag{24}$$

$$I_{source} = |I_{Load}| \tag{25}$$

A more accurate representation takes into account MOSFET, which practically presents a <1% difference in analysis. Later, this is connected to the WPT estimation, which considers sinusoidal input instead of square, hence

$$V_{square} = \sqrt{2}V_{sine} \tag{26}$$

3.3. Dynamic Wireless Power Transfer

To replace the WPT circuit, a power estimate from the secondary DC bus is used to estimate load resistance ($R_L = P_{DC2} / V_{REC}$). To incorporate the rectifier, an equivalent resistance is used to account for the rectified power consumption ($R_{eq} = 8R_L / \pi^2$). Likewise for the inverter voltage, a sinusoidal input is assumed in AC analysis ($V_{in} = V_{DC} \sin(f)$, where f is the operating frequency). The remaining variables represent compensation capacitors C1 and C2, coil inductance L1 and L2, and their resistance R1 and R2, the remaining parameter for mutual inductance links the primary and secondary sides. Note that the mutual inductance is calculated from a dimensionless parameter of the coupling factor (k), where $k = M\sqrt{L_1L_2}$. With all of the above parameters, a steady state value can be estimated for both the input and output current using the impedance at operating frequency f for all passive components.

$$Z_1 = R_1 + j\omega L_1 + 1/j\omega L_1 \tag{27}$$

$$Z_2 = R_2 + j\omega L_2 + 1/j\omega L_2 + R_{eq} \tag{28}$$

Voltage analysis of both sides gives

$$V_{DC} = i_1 Z_1 + j\omega M i_2 \tag{29}$$

$$j\omega M i_1 = Z_2 i_2 \tag{30}$$

Hence, the input and output current can be obtained as follows:

$$i_1 = V_{DC} / (Z_1 - \omega^2 M^2 / Z_2) \tag{31}$$

$$i_2 = i_1 * j\omega M / Z_2 \tag{32}$$

For dynamic charging, the steady state values will need to change as system parameters (such as coupling factor changes); hence, we are more interested in the peak values of V/I. To achieve this, we can use the total impedance of the system for the following differential equations:

$$\frac{d(i_1)}{dt} = \frac{V_{in} - i_1 \Re Z_1 - \omega M i_2}{\Im Z_1} \tag{33}$$

$$\frac{d(i_2)}{dt} = \frac{\omega M i_1 - i_2 \Re Z_2}{\Im Z_2} \tag{34}$$

Hence, we can relate primary and secondary DC buses based on input voltage and the output equivalent resistance. The full circuit features a dual active bridge, where the primary and secondary current values can be converted to the equivalent DC currents before the inverter and after rectification for i_1 and i_2 , respectively.

Hence, the WPT equivalent circuit implementation is shown in Figures 8 and 9. The MATLAB Simulink implementation code used to implement the aforementioned equations is shown in Appendices A and B.

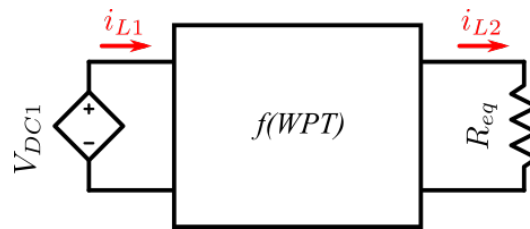


Figure 8. WPT equivalent circuit.

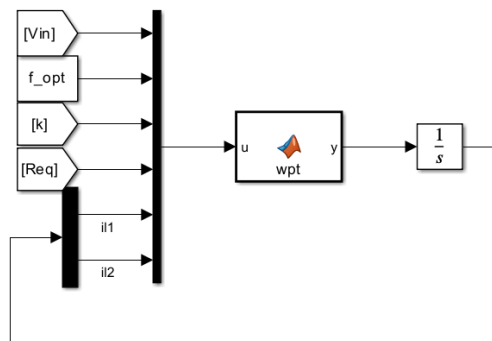


Figure 9. WPT Simulink implementation.

3.4. Semi-Controlled Rectifier

A semi-controlled rectifier is used to control rectifier voltage, switching off the input current from the WPT coil. For this function, the two MOSFETs are controlled to disconnect the power flow to the secondary DC converter.

Analysing the switching behaviour of the controlled rectifier, we find that the voltage before the rectifier is a function of the secondary coil current, rectified voltage and the rectifier diode/MOSFET on resistance, such that

$$d = 0 : V_s = V_{rec} * \text{sign}(I_s) + 2R_{fet}I_s \quad (35)$$

$$d = 1 : V_s = 2R_{fet}I_s \quad (36)$$

The current relationship is given by

$$d = 0 : I_s = I_c + I_L \quad (37)$$

$$d = 1 : 0 = I_c + I_L \quad (38)$$

Note that d denotes the duty cycle of the switching signal for the semi-controlled rectifier.

The approximation used for the proposed system is given by

$$dI_s = I_c + I_L \quad (39)$$

$$V_s = I_L^2 R_L / I_s \quad (40)$$

4. Results and Discussion

4.1. DC/DC Converter

The operation of DC/DC converters is not a novelty; hence, the main difference in switching direction is of interest. For this reason, a change from forward to reverse buck–boost mode is chosen to showcase the direction-switching capability. The main working principle is the inductor current switching from positive to negative to indicate the change in direction in current flow.

The results presented in Figure 10 show a comparison between the proposed model and switching model, where an accurate representation is achieved. Note that the switching model shows the resulting waveform from a simulation with a switching frequency of 2 kHz, compared to the simplified model utilising the proposed equivalent model based on system equations (i.e., it does not have a fixed frequency requirement). The equivalent circuit proposed is therefore able to reduce the simulation time to 1.03 s compared to the switching circuit's 3.54 s (see Table 2) required for the waveform seen in Figure 10, the steady state and rise time of each switching event is noted in Table 3.

Table 2. Comparison of simulation models.

Subsystem	Circuit	Frequency	Elapsed Time	Steady State Error
DC/DC converter	Switching model	2 kHz	3.54 s	1%
	Simplified model	N/A	1.03 s	
DWPT	Switching circuit	85 kHz	90.67 s	2.5%
	Simplified model	N/A	5.18 s	
Full circuit	Switching circuit	85 kHz	1061.47 s	6%
	Simplified model	N/A	30.97s	

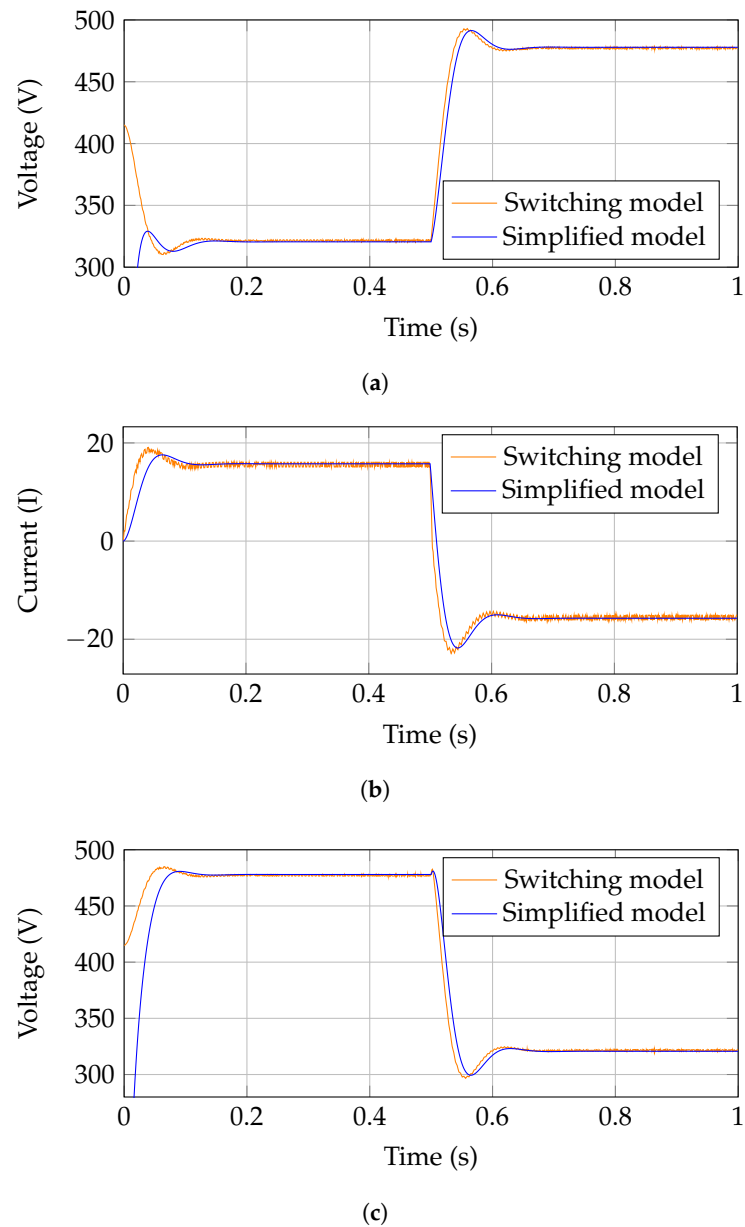


Figure 10. Bidirectional DC/DC converter switching from forward to reverse buck-boost mode at $t = 0.5$ s. (a) Voltage (V_{C1}) comparison. (b) Inductor current (I_L) comparison. (c) Voltage (V_{C2}) comparison.

Table 3. Comparison of DC/DC converter stay state values, error and delay between the switching and simplified models shown in Figure 10.

Variable	Switching Model	Simplified Model
Voltage V_{C1} (0–0.5 s)	321.5 (± 0.625)	320.5
Voltage V_{C1} (0.5–1 s)	477.25 (± 0.64)	477.9
Rise time (circa 0.1 s)	29 ms	36.1 ms
Rise time (circa 0.55 s)	27.9 ms	32.9 ms
Current I_L (0–0.5 s)	15.58 (± 0.478)	15.75
Current I_L (0.5–1 s)	−15.58 (± 0.478)	−15.72
Time delay (circa 0.05 s)	19 ms	30 ms
Time delay (circa 0.55 s)	12.1 ms	19.15 ms
Voltage V_{C1} (0–0.5 s)	477.26 (± 0.62)	478
Voltage V_{C1} (0.5–1 s)	321.49 (± 0.623)	320.68
Time delay (circa 0.55 s)	29.85 ms	40 ms
Time delay (circa 0.55 s)	23 ms	27.5 ms

4.2. Wireless Power Transfer

Validation of the proposed WPT equivalent circuit is shown in Figure 11 with steady state values for current amplitude at steady state note in Table 4. First, the system operation is shown at a steady state with a step change in the coupling factor. Then, the direction of power flow is reversed and the step change is reverted to show the system operating in reverse mode. Notably, the proposed system gives the peak value of primary and secondary currents, which normally remain 0; here, however, the magnitude is given as negative to indicate the direction of power flow.

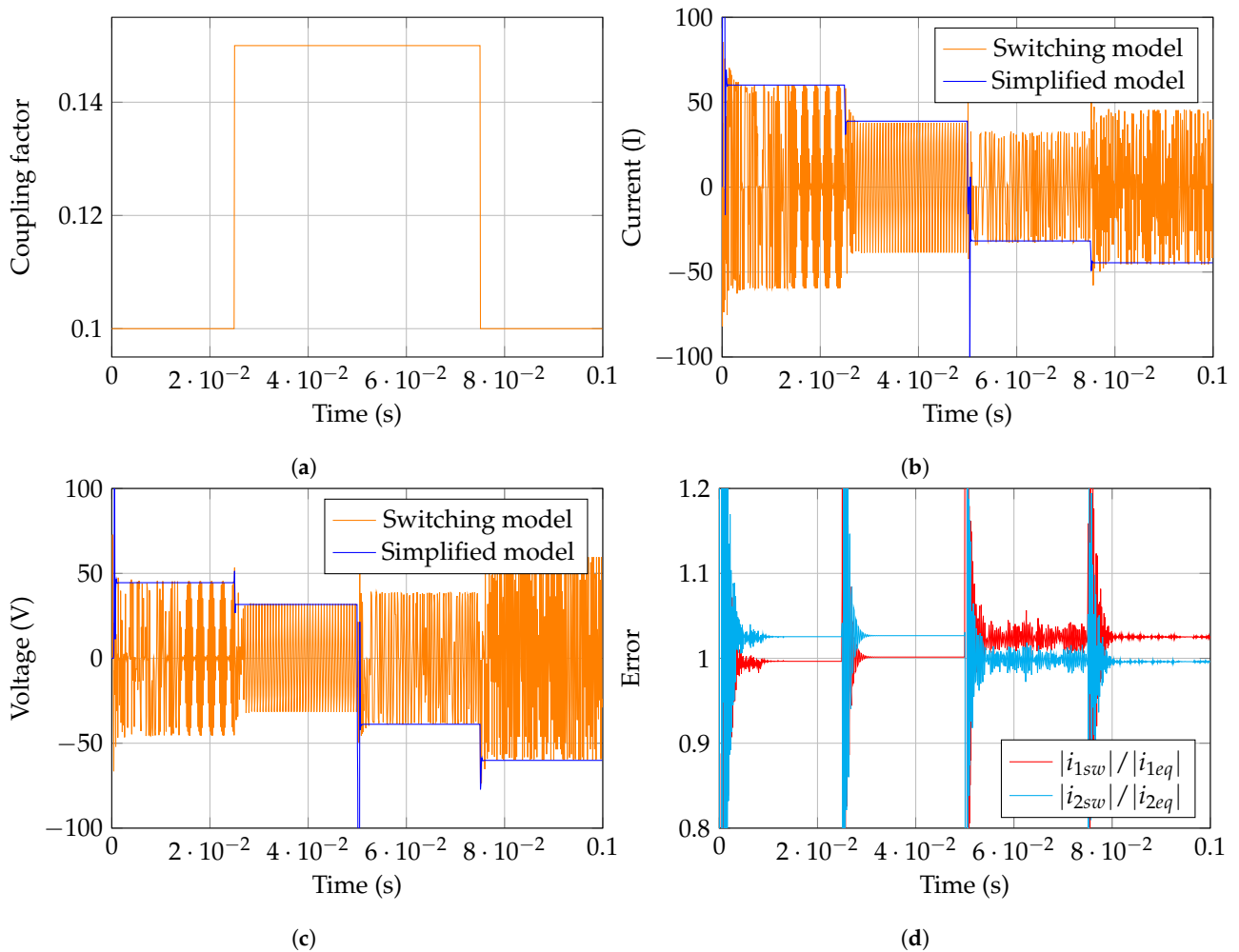


Figure 11. Comparisons of primary and secondary currents for bidirectional WPT, switching direction at 50 ms. (a) Coupling factor (k). (b) Primary coil current (i1). (c) Secondary coil current (i2). (d) Error comparison.

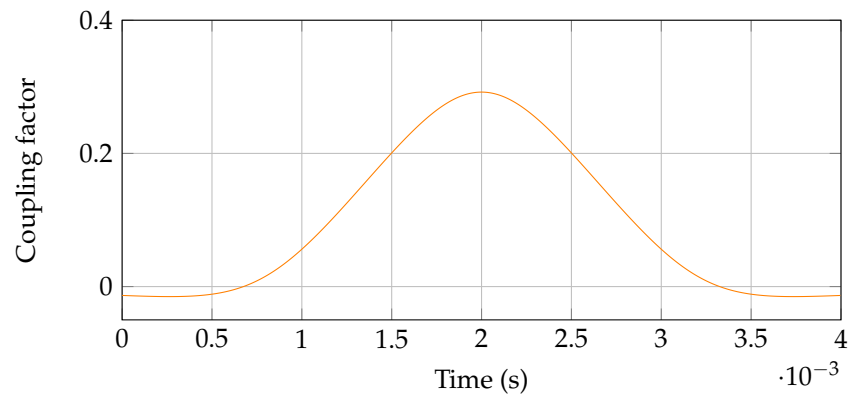
Both the switching and simplified models are provided with the same inputs, where the switching circuit shows the switching waveform at its operational frequency of 85 kHz, whereas the simplified model provides the envelope (magnitude) of this waveform. To compare the two more directly, a Fourier transform of the switching circuit is computed to obtain its magnitude; this can then be compared directly to the magnitude obtained from the simplified model. As the simplified model does not require high-frequency switching, it is able to reduce the switching model’s simulation time of 90.67 s down to 5.18 s (Table 2) for the equivalent circuit while capturing circuit dynamics.

Table 4. Stead-state current amplitude comparison at various time steps in Figure 11.

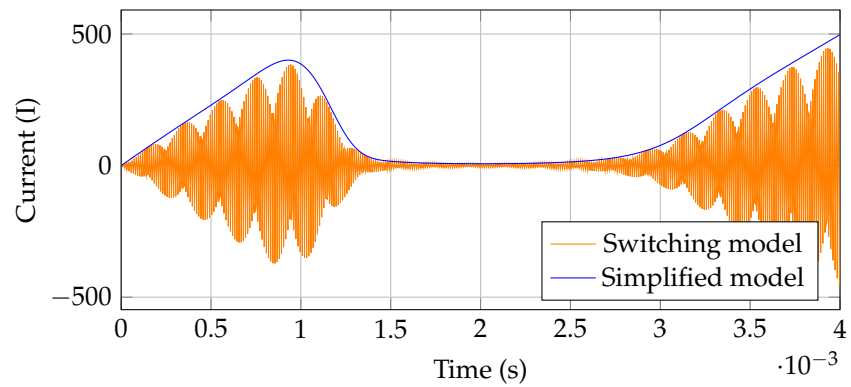
Variable	Switching Model	Simplified Model
Current i_1 (0–25 ms)	59.63	60.10
Current i_1 (25–50 ms)	38.65	38.84
Current i_1 (50–75 ms)	–32.25	–31.686
Current i_1 (75–100 ms)	–45.34	–44.52

4.3. Dynamic Wireless Power Transfer

Applying the WPT model to a dynamic scenario, Figure 12 shows the comparison of primary and secondary coil currents as a function of the coupling factor, where the direction of power flow is switched at 50 ms. The proposed system successfully estimates the magnitude of the coil current, which can then be used to connect to different subsystems (inverter and rectifier) for further analysis.

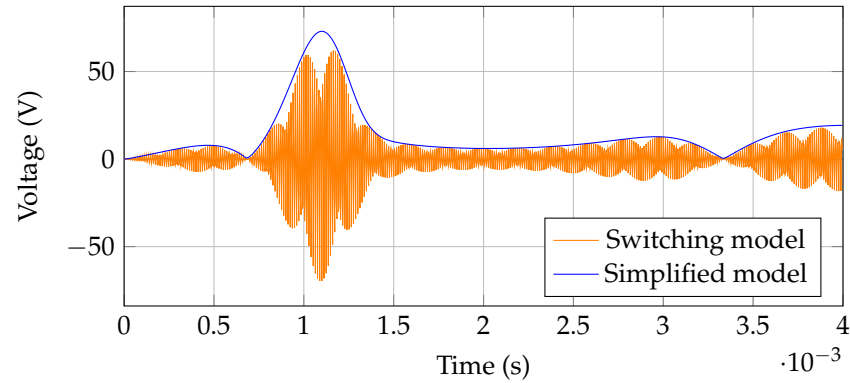


(a)



(b)

Figure 12. Cont.



(c)

Figure 12. Comparisons of primary and secondary currents for DWPT. (a) Coupling factor (k). (b) Primary coil current (i_1). (c) Secondary coil current (i_2).

4.4. Full System

The main point of interest for grid interaction simulations is the input (source) and output currents, which are shown in Figure 13. The results show a very similar dynamic response with the main variance being a phase shift in the input current. The proposed simulation captures the dynamic behaviour of the system at a much improved simulation time at the cost of a slight time inaccuracy. System parameters used are shown in Table 5.

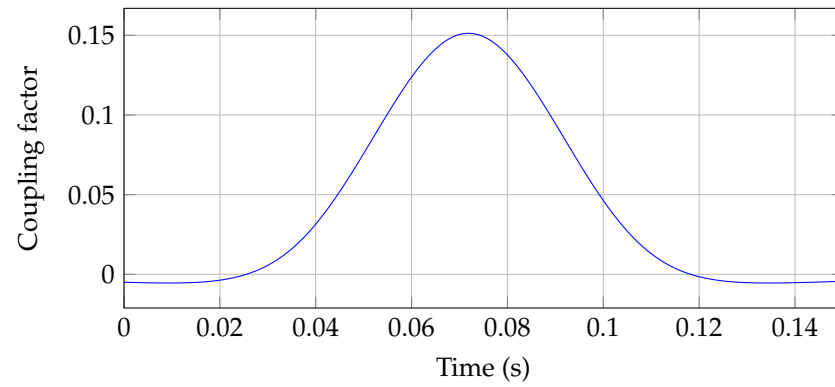
Table 5. Simulation system parameters.

Parameter	Symbol (s)	Value
Coil inductance	L_p, L_s	132.410 μH
Coil internal resistance	R_p, R_s	1.3 $\text{m}\Omega$
Compensation capacitance	C_p, C_s	26.477 μF
DC/DC converter inductance	L_{DCDC1}, L_{DCDC2}	5 mH
DC/DC converter capacitance	C_{DC1}, C_{rec}	1.5 mF
Inverter frequency	f_i	85 kHz
DC/DC converter frequency	f_{dc}	2 kHz

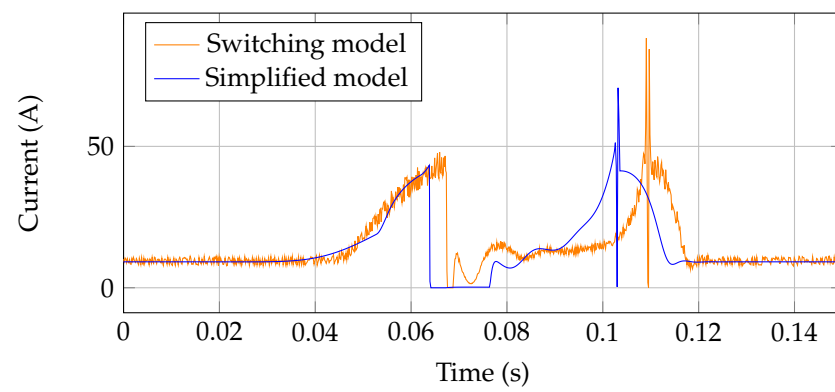
Further exploring the accuracy of the system, the DC bus voltages are shown in Figure 14, wherein again, a similar response is shown, with the main reference voltages being successfully obtained. Notably, the secondary DC voltage settles to a higher resting voltage, which is due to the simplification of the system not including all internal resistances, which would further reduce this value.

Comparing the energy consumption at the source gives a better estimation of accuracy, as it will settle down to an approximate value after the aforementioned time shift in results. Figure 15 shows this result, where the main working area can be seen at approximately between 5 ms to 12 ms; the error is higher due to the shift and lowers again after this period. Hence, as a charging event, the proposed system would give an accurate representation of energy consumption with a 10 ms difference.

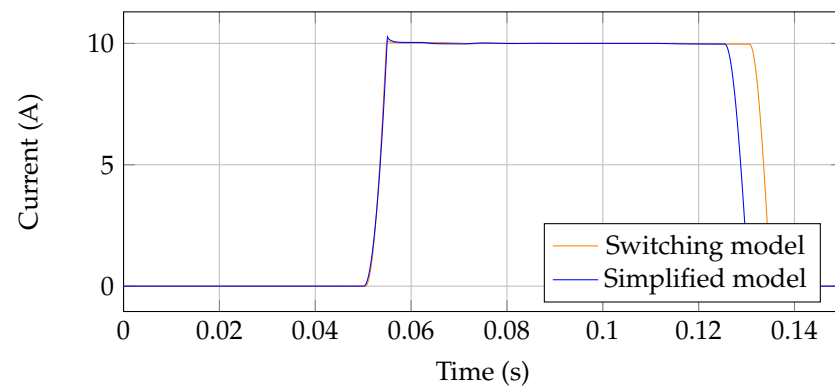
The time delay seen in Figures 13 and 15 are shown in Table 6.



(a)

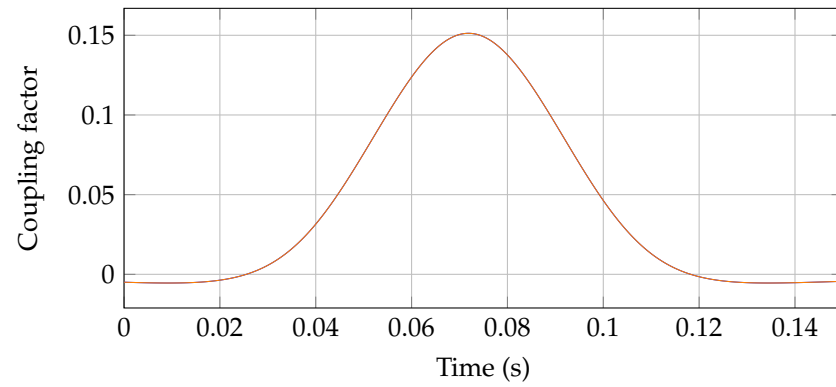


(b)

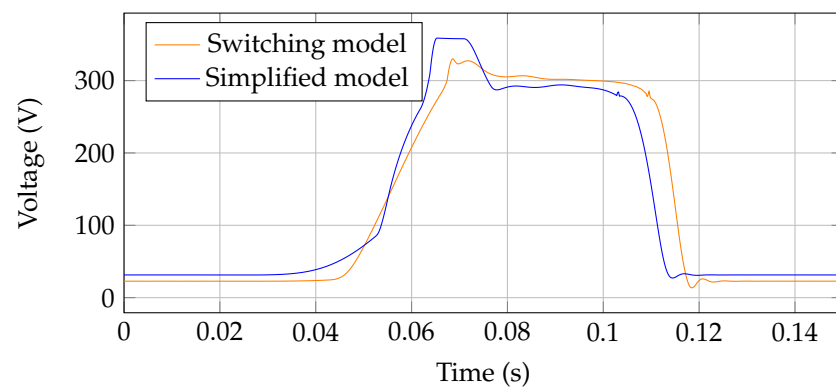


(c)

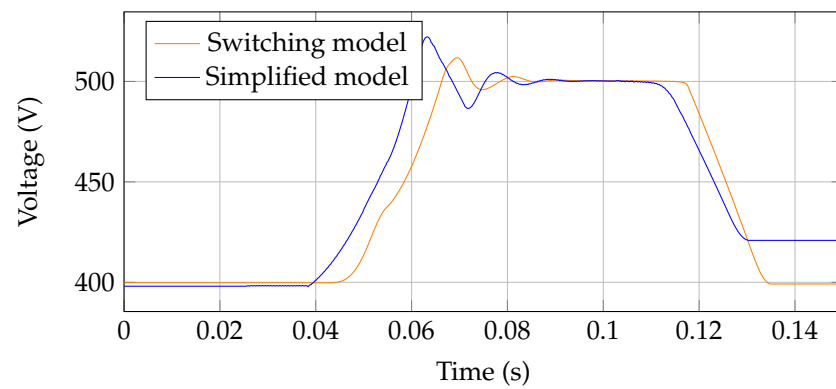
Figure 13. Full system input and output current comparison in a dynamic scenario. (a) Coupling factor (k). (b) Source current (i_{source}). (c) Output current (i_o).



(a)

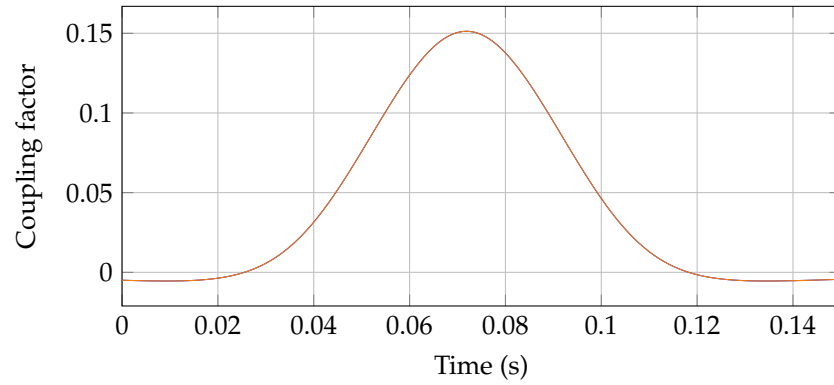


(b)

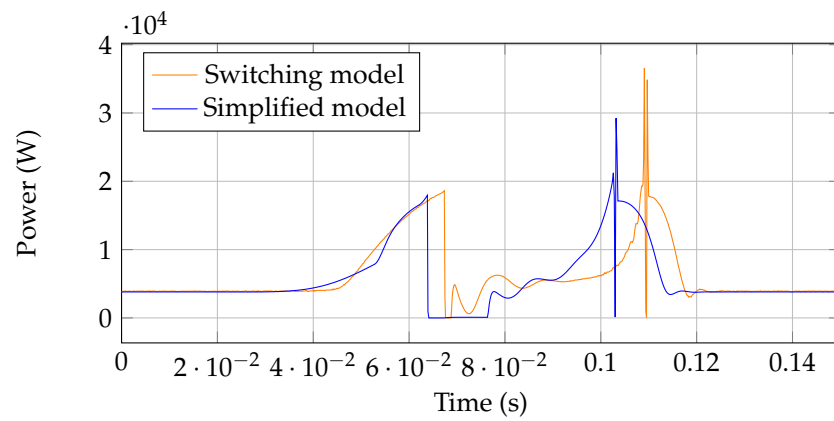


(c)

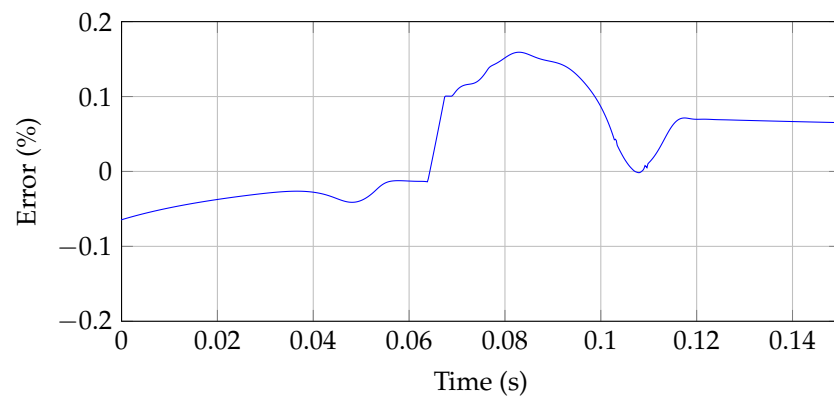
Figure 14. Full-system DC bus voltage comparison in a dynamic scenario. (a) Coupling factor (k). (b) Primary DC bus voltage (v_{DC1}). (c) Secondary DC bus voltage (v_{DC2}).



(a)



(b)



(c)

Figure 15. Full system power comparison and running error estimation. (a) Coupling factor (k). (b) Instantaneous source power. (c) Cumulative error ($\frac{\int P_{sw}}{\int P_{eq}}$).

Table 6. Notable time difference from Figures 13 and 15.

Variable	Figure and Estimated Time	Time Delay
i_{source} on delay	Figure 13b, circa 65 ms	5.468 ms
i_{source} off delay	Figure 13b, circa 110 ms	6.148 ms
i_o off delay	Figure 13c, circa 130 ms	4.489 ms
P_{source} on delay	Figure 15b, circa 65 ms	5.427 ms
P_{source} peak delay	Figure 15b, circa 110 ms	6.165 ms
V_{DC1} on delay	Figure 14b, circa 65 ms	5.688 ms
V_{DC1} off delay	Figure 14b, circa 110 ms	4.184 ms
V_{DC2} on delay	Figure 14c, circa 65 ms	7.529 ms
V_{DC2} off delay	Figure 14c, circa 110 ms	1.935 ms

4.5. Simulation Time

The system used for simulation has the following specifications: CPU—Intel i7-9700 @3.00GHz; Memory—16 GB RAM; OS—Windows 11 64-bit (10.0 Build); Matlab—R2023a.

Table 2 shows a comparison of the simulation times for each circuit presented. Notably, the main simulation showed a $34\times$ reduction in simulation time for the same simulation duration, confirming the effectiveness of the simulation techniques in reducing simulation time.

The increased simulation time is due to the increased complexity of the full circuit model and computation required to obtain the results. This is also true for the proposed equivalent circuit; however, instantaneous values for the voltage/current are omitted, which in turn allows for an increase in the required time step to obtain the results.

5. Conclusions

This paper first presented the DWC and the average modelling techniques used to capture circuit dynamics while reducing simulation time by removing high-frequency switching components. Notably, the lower-frequency DC/DC converter (2 kHz) shows a smaller time improvement over the high frequency (85 kHz) required for DWPT. The proposed modelling method successfully reduced simulation time for the DWPT model, reducing simulation time by a factor of 30. The main circuit for WPT showed a speed improvement by a factor of 17 while maintaining accuracy within a 2.5% error, which is suitable for the application. Further expansion to a more complex circuit introduced complications which reduced accuracy; however, the modelling techniques used still proved to be useful in reducing the computation time. The proposed circuit will be able to connect to standard-power-factor-correction circuits or grid-connected converters.

Additionally, the implementation splits the whole circuit into the main components of DC converters and the DWPT model, where duty cycle values are used to implement the system control. This allows for future work involving system controls, focused on reducing power consumption without a vehicle connection. This approach also allows for replacing subsystems based on future developments in the field.

6. Future Work

6.1. Inverter/Rectifier Model Improvements

The main issue with the implementation was observed to be the interconnection of subsystems. In fact, the issue of this interconnection is the subsystem behaviour with a low coupling factor (for WPT). This proved to be an issue with the controlled rectifier as at this time, the power supplied to the output was approximately zero, meaning its resistance was effectively infinite. Hence, further study of this interaction would be useful; alternatively, expanding the circuit analysis into that which is made up of one whole system instead of comprising separate subsystems is also possible.

6.2. Multiple-Coil Systems

Expanding the circuit to accommodate multiple-coil systems, both primary and secondary, represents a significant advancement in research, as we move towards including multiple vehicles for charging and integrating multiple transmitter coils. This approach will allow for more comprehensive investigations into practical implementations of DWPT technology. Simulating multiple primary coils with a vehicle travelling between them is a logical next step, as it more accurately reflects future scenarios where road sections are electrified with several transmitter coils. This will also enhance the relevance of grid integration studies.

In order to expand the system for multiple coils, the mutual inductance link between coils is required, followed by their associated circuitry (for primary coils, the DC converter and inverter are needed, and vice versa for secondary coils). Linking the coils to other coils in the system requires updating the induced Electromagnetic Field (EMF) on each coil. This has been considered in the selection of modelling methods for WPT, where Equation (34) is

updated with the current and mutual inductance of other coils. Note that to expand the system, each coil should have a link to all other coils for accuracy.

6.3. Integration into Grid Systems

The proposed system is analysed with a DC power supply where the voltage reading is fed into the system for analysis and the system provides a current draw depending on the system dynamics. To integrate the system into other systems such as grid simulations, the DC supply can be replaced by a DC grid connection; otherwise, a rectified grid connection can also be used to provide the DC link for the system. From there, the current draw will act as a load for the system.

Author Contributions: Conceptualization, K.J. and C.L.; methodology, K.J., C.L. and J.L.; software, K.J.; validation, J.L., L.C. and C.L.; formal analysis, K.J.; investigation, K.J.; resources, J.L., L.C. and J.W.; data curation, K.J.; writing—original draft preparation, K.J.; writing—review and editing, K.J.; visualization, K.J.; supervision, J.L., L.C., C.L.; project administration, K.J.; funding acquisition, J.W. All authors have read and agreed to the published version of the manuscript.

Funding: This research was funded by EPSRC as part of K. Jakubiak's PhD studentship.

Data Availability Statement: Data are contained within the article.

Conflicts of Interest: The authors declare no conflict of interest.

Appendix A. DC/DC Converter cCode

```
function y = Buck(u)
% Input signals
Vs = u (1);      % input voltage
i1 = u (2);      % input current
i2 = u (3);      % output current (measurement)
d = u (4);       % duty cycle
mode = u (5);    % switching frequency
vc1 = u (6);     % capacitor 1 voltage
iL = u (7);      % inductor current
vc2 = u (8);     % capacitor 2 voltage

% Circuit parameters
L = 0.005;       % inductance
C1 = 0.0015;     % output capacitance
C2 = 0.0015;     % output capacitance

%(iL*.05 + i2*.05) dampens the output using "on" resistance of components

switch mode
    case 1 %Buck
        dvc1 = (i1-d*iL)/C1;
        dil = (d*vc1-vc2 - (iL*.05 + i2*.05))/L;
        dvc2 = (iL-i2)/C2;

    case 2 %Buck-boost
        dvc1 = (i1-d*iL)/C1;
        dil = (d*vc1-vc2*(1-d)-(iL*.05 + i2*.05))/L;
        dvc2 = ((1-d)*iL-i2)/C2;

    case 3 %boost
        dvc1 = (i1-iL)/C1;
        dil = (vc1-vc2*(1-d)-(iL*.05 + i2*.05))/L;
```

```

        dvc2 = ((1-d)*iL-i2)/C2;

    case 4 %reverse buck
        dvc1 = (i1-iL)/C1;
        dil = (vc1-d*vc2 - (iL*.05 + i2*.05))/L;
        dvc2 = (d*iL-i2)/C2;

    case 5
        dvc1 = (i1-(1-d)*iL)/C1;
        dil = (vc1*(1-d)-d*vc2-(iL*.05 + i2*.05))/L;
        dvc2 = (d*iL-i2)/C2;

    case 6
        dvc1 = (i1-(1-d)*iL)/C1;
        dil = (vc1*(1-d)-vc2-(iL*.05 + i2*.05))/L;
        dvc2 = (iL-i2)/C2;

    otherwise
        disp('error');
        dvc1 =0;
        dil =0;
        dvc2 =0;
end

% Output results
y = [dvc1 dil dvc2];

```

Appendix B. WPT Converter Code

```

function [y,i2est] = fcn(u)
%% Define input from mux. (u)
mode = u (1); %v2g mode
Vin1 = u (2);
Vin2 = u (4);
RL = u (5);
f = u (6);
k = abs(u (7));
il1 = u (9);
il2 = u (10);

% Coil self inductance & resistance
L1 = 1.3241e-04;
R1 = 1.3e-3;
L2 = 1.3241e-04;
R2 = 1.3e-3;
% Compensation capacitor
C1 = 2.6477e-08;
C2 = 2.6477e-08;
M = k*sqrt(L1*L2); % k=0.1
w = 2*pi*f;

Rfet =0.1;

```

```

sf = 8;
RL = RL* 8/pi^2;

switch mode
    case 1 % reverse mode
        Z1 = RL + R1 + 1j*w*(L1) + 1/(1j*w*C1) + 2*Rfet;
        Z2 = R2 + 1j*w*(L2) + 1/(1j*w*C2) + 2*Rfet;
        dil1 = (w*M*il2 - il1*real(Z1))/abs(imag(Z1)/sf);
        dil2 = (-1.27*Vin1 - w*M*il1 - real(Z2)*il2)/abs(imag(Z2)/sf);

    otherwise % Forward mode
        Z1 = R1 + 1j*w*(L1) + 1/(1j*w*C1) + 2*Rfet;
        Z2 = RL + R2 + 1j*w*(L2) + 1/(1j*w*C2) + 2*Rfet;
        dil1 = (1.27*Vin1 - il1*real(Z1) - w*M*il2)/abs(imag(Z1)/sf);
        dil2 = (w*M*il1 - real(Z2)*il2)/abs(imag(Z2)/sf);

end

% Secondary coil current (i2) estimation at steady state
i1 = Vin1/(Z1-w^2*M^2/Z2);
i2 = i1*w*M/Z2;
i2est = abs(i2);

y = [dil1, dil2];

```

References

1. Our World in Data. Emissions by Sector—Our World in Data. Available online: <https://ourworldindata.org/emissions-by-sector> (accessed on 15 June 2023).
2. Kumar, M.; Panda, K.P.; Naayagi, R.T.; Thakur, R.; Panda, G. Comprehensive Review of Electric Vehicle Technology and Its Impacts: Detailed Investigation of Charging Infrastructure, Power Management, and Control Techniques. *Appl. Sci.* **2023**, *13*, 8919. [\[CrossRef\]](#)
3. Dimitriadou, K.; Rigogiannis, N.; Fountoukidis, S.; Kotarela, F.; Kyritsis, A.; Papanikolaou, N. Current trends in electric vehicle charging infrastructure; opportunities and challenges in wireless charging integration. *Energies* **2023**, *16*, 2057. [\[CrossRef\]](#)
4. Machura, P.; Li, Q. A critical review on wireless charging for electric vehicles. *Renew. Sustain. Energy Rev.* **2019**, *104*, 209–234. [\[CrossRef\]](#)
5. Mude, K.N.; Aditya, K. Comprehensive review and analysis of two-element resonant compensation topologies for wireless inductive power transfer systems. *Chin. J. Electr. Eng.* **2019**, *5*, 14–31. [\[CrossRef\]](#)
6. Miller, J.M.; Jones, P.; Li, J.M.; Onar, O.C. ORNL Experience and Challenges Facing Dynamic Wireless Power Charging of EV's. *IEEE Circuits Syst. Mag.* **2015**, *15*, 40–53. [\[CrossRef\]](#)
7. Mou, X.; Gladwin, D.T.; Zhao, R.; Sun, H. Survey on magnetic resonant coupling wireless power transfer technology for electric vehicle charging. *IET Power Electron.* **2019**, *12*, 3005–3020. [\[CrossRef\]](#)
8. Song, K.; Koh, K.E.; Zhu, C.; Jiang, J.; Wang, C.; Huang, X. A Review of Dynamic Wireless Power Transfer for In-Motion Electric Vehicles. In *Wireless Power Transfer*; Coca, E., Ed.; IntechOpen: Rijeka, Hrvatska, 2016; Chapter 6. [\[CrossRef\]](#)
9. Song, B.; Cui, S.; Li, Y.; Zhu, C. A Narrow-Rail Three-Phase Magnetic Coupler With Uniform Output Power for EV Dynamic Wireless Charging. *IEEE Trans. Ind. Electron.* **2021**, *68*, 6456–6469. [\[CrossRef\]](#)
10. Park, C.; Lee, S.; Jeong, S.Y.; Cho, G.H.; Rim, C.T. Uniform Power I-Type Inductive Power Transfer System With DQ-Power Supply Rails for On-Line Electric Vehicles. *IEEE Trans. Power Electron.* **2015**, *30*, 6446–6455. [\[CrossRef\]](#)
11. Song, S.; Zhang, Q.; He, Z.; Li, H.; Zhang, X. Uniform Power Dynamic Wireless Charging System With I-Type Power Supply Rail and DQ-Phase-Receiver Employing Receiver-Side Control. *IEEE Trans. Power Electron.* **2020**, *35*, 11205–11212. [\[CrossRef\]](#)
12. Sallan, J.; Villa, J.L.; Llombart, A.; Sanz, J.F. Optimal Design of ICPT Systems Applied to Electric Vehicle Battery Charge. *IEEE Trans. Ind. Electron.* **2009**, *56*, 2140–2149. [\[CrossRef\]](#)
13. Zhang, X.; Meng, H.; Wei, B.; Wang, S.; Yang, Q. Mutual inductance calculation for coils with misalignment in wireless power transfer. *J. Eng.* **2019**, *2019*, 1041–1044. [\[CrossRef\]](#)
14. Su, Y.P.; Liu, X.; Hui, S.Y.R. Mutual Inductance Calculation of Movable Planar Coils on Parallel Surfaces. *IEEE Trans. Power Electron.* **2009**, *24*, 1115–1123. [\[CrossRef\]](#)
15. Cheng, Y.; Shu, Y. A New Analytical Calculation of the Mutual Inductance of the Coaxial Spiral Rectangular Coils. *IEEE Trans. Magn.* **2014**, *50*, 1–6. [\[CrossRef\]](#)

16. Li, Z.; Zhang, M. Mutual inductance calculation of circular coils arbitrary positioned with magnetic tiles for wireless power transfer system. *IET Power Electron.* **2020**, *13*, 3522–3527. [[CrossRef](#)]
17. Zhang, X.; Quan, C.; Li, Z. Mutual Inductance Calculation of Circular Coils for an Arbitrary Position With Electromagnetic Shielding in Wireless Power Transfer Systems. *IEEE Trans. Transp. Electrification.* **2021**, *7*, 1196–1204. [[CrossRef](#)]
18. Dehui, W.; Fan, Y.; Chao, H.; Fang, C. Method for the calculation of coupling coefficient between two arbitrary-shaped coils. *IET Power Electron.* **2019**, *12*, 3936–3941. [[CrossRef](#)]
19. Nawaz, B. Analytical Calculation of the Coupling Factor for Single and Multi-layered Circular, Square, and Hexagonal Wireless Power Transfer Coils. In Proceedings of the 2020 IEEE Wireless Power Transfer Conference (WPTC), Seoul, Republic of Korea, 15–19 November 2020; pp. 453–459. [[CrossRef](#)]
20. Mendes Duarte, R.; Klaric Felic, G. Analysis of the Coupling Coefficient in Inductive Energy Transfer Systems. *Act. Passiv. Electron. Compon.* **2014**, *2014*, 951624. [[CrossRef](#)]
21. Zhang, X.; Yuan, Z.; Yang, Q.; Li, Y.; Zhu, J.; Li, Y. Coil design and efficiency analysis for dynamic wireless charging system for electric vehicles. *IEEE Trans. Magn.* **2016**, *52*, 1–4. [[CrossRef](#)]
22. Tavakoli, R.; Pantic, Z. Analysis, design, and demonstration of a 25-kW dynamic wireless charging system for roadway electric vehicles. *IEEE J. Emerg. Sel. Top. Power Electron.* **2017**, *6*, 1378–1393. [[CrossRef](#)]
23. Tan, L.; Zhao, W.; Liu, H.; Li, J.; Huang, X. Design and optimization of ground-side power transmitting coil parameters for EV dynamic wireless charging system. *IEEE Access* **2020**, *8*, 74595–74604. [[CrossRef](#)]
24. Cui, S.; Wang, Z.; Han, S.; Zhu, C.; Chan, C. Analysis and design of multiphase receiver with reduction of output fluctuation for EV dynamic wireless charging system. *IEEE Trans. Power Electron.* **2018**, *34*, 4112–4124. [[CrossRef](#)]
25. Bagchi, A.C.; Kamineni, A.; Zane, R.A.; Carlson, R. Review and Comparative Analysis of Topologies and Control Methods in Dynamic Wireless Charging of Electric Vehicles. *IEEE J. Emerg. Sel. Top. Power Electron.* **2021**, *9*, 4947–4962. [[CrossRef](#)]
26. Tan, L.; Zhao, W.; Ju, M.; Liu, H.; Huang, X. Research on an EV dynamic wireless charging control method adapting to speed change. *Energies* **2019**, *12*, 2214. [[CrossRef](#)]
27. Jakubiak, K.; Liang, J.; Cipcigan, L. Modelling of inductive wireless charging for electric vehicles. In Proceedings of the 2022 IEEE 16th International Conference on Compatibility, Power Electronics, and Power Engineering (CPE-POWERENG), Birmingham, UK, 29 June–1 July 2022; IEEE: Piscataway, NJ, USA, 2022; pp. 1–7.
28. Jakubiak, K.; Li, C.; Liang, J.; Cipcigan, L. Control & modelling of wireless charging system for electric vehicles and their application in dynamic scenarios. In Proceedings of the EVI: Charging Ahead (EVI 2023), Glasgow, UK, 14–17 November 2023; IET: London, UK, 2023; Volume 2023, pp. 7–14.
29. Choi, W.K.; Park, C.W.; Lee, K. Circuit analysis of achievable transmission efficiency in an overcoupled region for wireless power transfer systems. *IEEE Syst. J.* **2017**, *12*, 3873–3876. [[CrossRef](#)]

Disclaimer/Publisher’s Note: The statements, opinions and data contained in all publications are solely those of the individual author(s) and contributor(s) and not of MDPI and/or the editor(s). MDPI and/or the editor(s) disclaim responsibility for any injury to people or property resulting from any ideas, methods, instructions or products referred to in the content.